NANO LETTERS

Letter

pubs.acs.org/NanoLett

Efficient Excitation of Channel Plasmons in Tailored, UV-Lithography-Defined V-Grooves

Cameron L. C. Smith,[†] Anil H. Thilsted,[†] Cesar E. Garcia-Ortiz,[‡] Ilya P. Radko,[‡] Rodolphe Marie,[†] Claus Jeppesen,[§] Christoph Vannahme,[†] Sergey I. Bozhevolnyi,[‡] and Anders Kristensen*[,†]

[†]Department of Micro- and Nanotechnology, Technical University of Denmark, DK-2800 Kongens Lyngby, Denmark

[‡]Institute of Technology and Innovation (ITI), University of Southern Denmark, DK-5230 Odense M, Denmark

[§]Department of Photonics Engineering, Technical University of Denmark, DK-2800 Kongens Lyngby, Denmark

ABSTRACT: We demonstrate the highly efficient (>50%) conversion of freely propagating light to channel plasmon-polaritons (CPPs) in gold V-groove waveguides using compact 1.6 μm long waveguide-termination coupling mirrors. Our straightforward fabrication process, involving UV-lithography and crystallographic silicon etching, forms the coupling mirrors innately and ensures exceptional-quality, wafer-scale device production. We tailor the V-shaped profiles by thermal silicon oxidation in order to shift initially wedge-located modes downward into the V-grooves, resulting in well-confined CPPs suitable for nanophotonic applications.

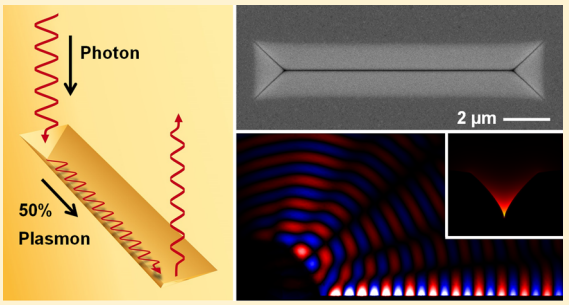

KEYWORDS: *Channel plasmon polariton, V-groove, termination mirror, plasmonic coupler, UV lithography*

Waveguide configurations based on surface plasmon-polaritons (SPPs) possess unique scaling properties that allow one to concentrate light beyond the diffraction limit.[1−5] This unique feature of SPP-based waveguides along with ongoing advances in fabrication technology has signaled the possibility of developing a new generation of subwavelength-integrated optical waveguides,[6−10] circuits,[11,12] and devices.[13−15] Accordingly, V-shaped grooves in metals supporting channel plasmon-polaritons (CPPs)[16] represent a particularly promising plasmonic waveguide configuration by providing a competitive confinement-loss trade-off in addition to efficient broadband transmission around sharp bends.[17,18] As a result, V-groove-supported CPPs have enabled the demonstration of ultracompact plasmonic circuit components[19,20] and novel nanofocusing elements.[21,22] However, the viability of plasmonic V-grooves for significant implementation requires a convenient approach to efficiently excite the CPP modes, that is, bridging the photon-plasmon momentum mismatch,[1] that can be realized with affordable fabrication techniques.[23−25]

To date, CPP excitation has typically involved end-fire coupling,[16] a method that requires a cleaved sample end-facet after fabrication. Sample cleaving is a cumbersome procedure that deteriorates the quality of the waveguide entrance and leaves it prone to further damage. Moreover, end-fire coupling requires the use of finely tapered polarization-maintaining single-mode optical fibers, where the coupling efficiency is critically and uniquely sensitive to their position and orientation. This problem applies in general to SPP-based waveguide configurations and has motivated the investigation of numerous directional nanoantenna configurations to conveniently launch plasmons via normally incident light, such as Yagi-Uda design,[26−28] single element,[29,30] phase-engineered,[31] nanopatch,[32,33] and Bragg resonator type arrangements.[34,35] Such SPP launchers avoid the need for cleaving procedures, maintain the mobility of device samples and locally excite the plasmon modes. Their merits may be further assessed by combining coupling efficiencies and compactness with particularly impressive results from Baron et al. (52% in-coupling, 8 μm long Bragg resonator)[35] and Kriesch et al. (45% in-coupling, 60% out-coupling, 1 μm^2 Yagi-Uda design antenna).[28] Recently, Radko et al. developed a coupling arrangement to excite V-groove-supported CPPs via normally incident illumination by tapering the waveguide terminations to form angled nanomirrors.[36] These nanomirrors facilitated the unidirectional launching of CPPs into nanoscale V-groove waveguides and occupied only subwavelength dimensions, although the maximum in-coupling efficiency was ∼10% and like the arrangements mentioned above required an expensive and time-consuming fabrication method such as focused ion beam (FIB) milling or electron beam lithography (EBL).

In this Letter, we demonstrate the experimental excitation of V-groove-supported CPPs with an in-coupling efficiency of over 50% using freely propagating light directed at normal incidence onto waveguide termination mirrors. The compact termination mirrors are 1.6 μm in length along the V-groove axis, each occupying a total planar area of ∼5.2 μm^2. The fabricated V-grooves and termination mirrors are both defined during the same conventional UV-lithography step which, combined with chemical etching of silicon crystallographic

Received: January 17, 2014

ACS Publications © XXXX American Chemical Society

dx.doi.org/10.1021/nl5002058 | *Nano Lett.* XXXX, XXX, XXX−XXX

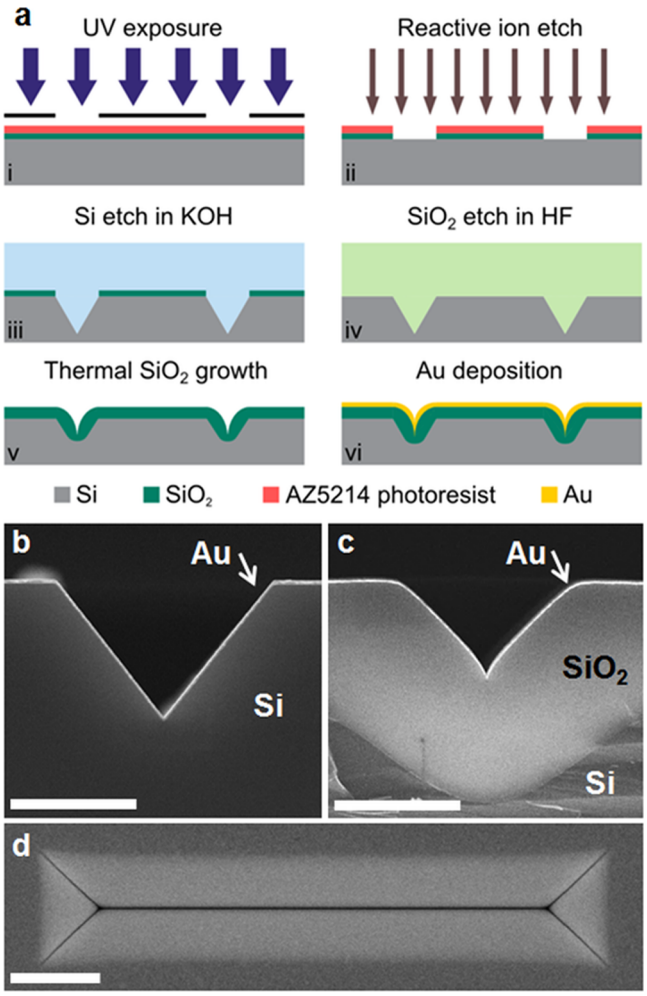

Figure 1. (a) The fabrication procedure for forming the gold V-grooves. UV-lithography together with a subsequent crystallographic etch in a KOH bath define the V-grooves and termination mirrors simultaneously. A thermal oxidation process is performed to modify the resulting V-groove profile before the gold layer (70 nm) is deposited. (b–d) SEM images of the resulting V-grooves, all scale bars are 2 μm. (b) Cross-section of a V-groove without thermal oxidation of the silicon substrate. (c) Cross-section of a V-groove with the thermal oxidation step. The SiO_2 thickness at flat sections of the substrate is 2320 nm. (d) Top-view of a V-groove waveguide with crystallographically formed termination mirrors. The profile has been modified by a thermal SiO_2 layer similar to the case in (c).

planes, forms the reproducible, high-quality profiles innately in a parallel, wafer-scale process. The silicon V-groove cross sections are tailored by thermal oxidation of the silicon substrate (before metal deposition) to sharpen the groove angle in order to ensure the existence of well-confined CPP modes. The experimental observations, coupling efficiencies and cross section tailoring, are supported by finite element method (FEM) calculations.

The fabrication procedure of our gold V-grooves waveguides and termination mirrors is depicted in Figure 1a. The process is improved upon previous works,[23−25] here involving conventional UV-lithography and a thermally grown silicon dioxide (SiO_2) layer on silicon to modify the V-shape geometry. Initially, a 200 nm SiO_2 layer on the silicon substrate is patterned by both UV-lithography and reactive ion etching to define the perimeter of the V-groove devices. The V-grooves

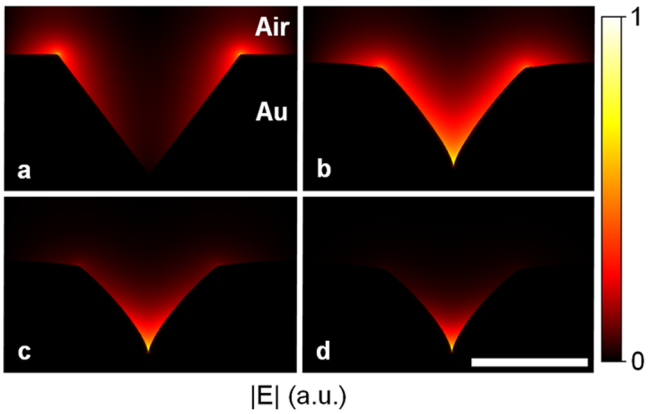

Figure 2. The 2D FEM calculations of the magnitude of the electric field solutions to varying V-groove cross sections in gold for λ_0 = 811 nm. (a) Zero oxidation. In this case, only modes located at the wedges exist; (b) 1320 nm oxidation; (c) 1720 nm oxidation; and (d) 2320 nm oxidation. It is evident that thicker SiO_2 layers lead to sharper V-shaped profiles resulting in increased confinement of the electric field distribution toward the bottom of the waveguide. A clear CPP mode can be identified in the case for (d). The scale bar is 2 μm.

and termination mirrors are formed by anisotropic wet etching of the exposed silicon in a potassium hydroxide (KOH) bath at 80 °C. The KOH etch yields smooth ⟨111⟩ V-groove sidewalls and termination mirrors with a fixed inclination of 55° from the surface plane. Curvature rounding of the V-groove perimeter during the UV step, which may be up to several hundred nanometers from features inherent to the UV mask or through processing steps, nevertheless yields excellent mirror formation due to the nature of the crystallographic etch. It is necessary that the patterning of the SiO_2 layer is well-aligned with the crystal ⟨100⟩ planes of the silicon substrate. The remaining SiO_2 is removed by etching in a hydrofluoric (HF) acid bath. Tailoring of the V-shape geometry is performed by thermal wet oxidation of the silicon V-grooves at 1150 °C for 9 h, resulting in a 2320 nm thick SiO_2 layer at flat sections of the substrate. The V-groove widths are 3.5 ± 0.1 μm before thermal oxidation and 3.2 ± 0.1 μm at the extreme edges after. Scanning electron microscope (SEM) images of device cross sections with and without the oxidation step are shown in Figure 1b,c. The metal is deposited by electron beam evaporation: first a 5 nm layer of chromium to promote adhesion before the 70 nm layer of gold. The gold layer is chosen to be sufficiently thick to eliminate interaction of air−interface plasmons with the SiO_2 layer and to also minimize aggregation. A SEM image of a complete device is shown in Figure 1d with a total length, including mirrors, of 16 μm.

The device design is performed via two-dimensional (2D) FEM calculations in COMSOL at a free space wavelength of λ_0 = 811 nm. The magnitude of the electric field distributions for fundamental plasmonic V-groove modes are plotted in Figure 2, corresponding to devices of varying SiO_2 layer thickness: (a) 0, (b) 1320, (c) 1720, and (d) 2320 nm. To represent the thermal oxidation step, the cross-section profiles are generated by numerical process simulations in ATHENA.[37] The numerically derived profiles enable predictions of the electric field distribution to be made and also yield finer detail in proximity to the bottom of the V-groove than SEM images can provide. A 5 nm radius of curvature is further introduced to the bottom of the V-shape to address real-world feature rounding and avoid computation singularities; this value is

dx.doi.org/10.1021/nl5002058 | Nano Lett. XXXX, XXX, XXX−XXX

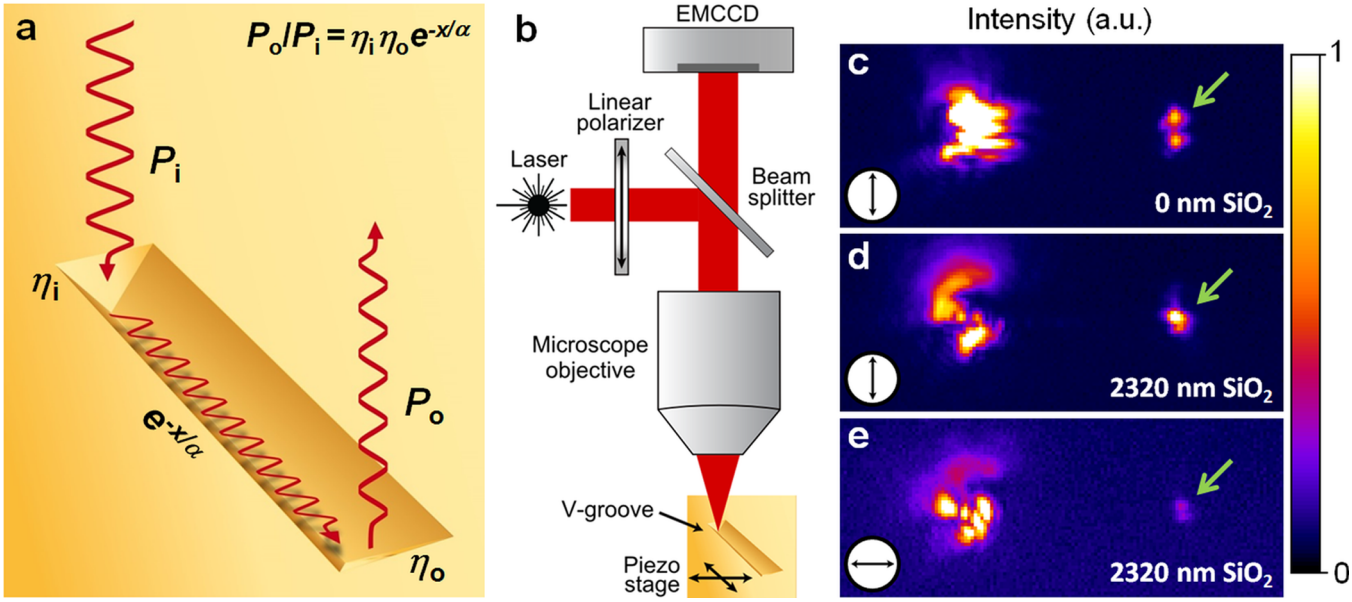

Figure 3. (a) Illustration of the in- and out-coupling of light via the V-groove plus termination-mirrors configuration. (b) Scheme of the experimental setup. Light from a laser diode (λ_0 = 811 nm) is linearly polarized before impinging onto the sample through a microscope objective. Detection is performed using an EMCCD camera and the sample is positioned via an *XY*-controlled piezoelectric stage. (c–e) Experimentally observed radiation from the out-coupling termination mirrors at the ends of 12.5 μm-length V-groove waveguides. The larger left spots are the direct reflection from the incident beam and the right spots are out-coupled light from the termination mirrors (indicated by arrows). Insets at the bottom left of the images represent the polarization of the incident electric field. The intensity range is normalized to the same input power for the images. (c) A pair of intensity peaks corresponding to a wedge mode pair can be observed for a V-groove device without oxidation. (d) A single intensity peak corresponding to a CPP mode is out-coupled from a V-groove device with a 2320 nm SiO_2 layer. The incident light polarization closely matches the electric field of the CPP and allows for efficient in-coupling. (e) A low out-coupled intensity occurs for the same device in (d) when the incident light polarization is rotated 90° and no longer matches the electric field of the CPP, resulting in a weak in-coupling efficiency and degeneracy of the out-coupled radiation.

supported by measurement-calculation comparisons. In Figure 2a, it is evident that only wedge-based modes exist for the case without oxidation. In Figure 2b–d, a thermally grown SiO_2 layer is shown to lead to a modified geometry with sharper V-shaped profiles and subsequently increased confinement of the electric field distribution toward the bottom of the waveguide. A well-defined CPP mode can be observed for the case of largest SiO_2 thickness in Figure 2d.

An illustration of the experimental configuration is shown in Figure 3a, portraying the optical path of light in the V-groove devices. The output-to-input signal ratio can be expressed as $P_o/P_i = \eta_i \eta_o e^{-x/\alpha}$ where η_i and η_o are the in-coupling and out-coupling efficiencies and α corresponds to the propagation length (1/loss) of the CPP intensity along the V-groove waveguide. To characterize the V-groove modes and coupling efficiencies we use the optical setup sketched in Figure 3b. The emission from a monochromatic continuous-wave fiber-coupled diode laser at a free space wavelength of λ_0 = 811 nm (full width at half-maximum (fwhm) = 0.3 nm) is guided into the optical path of an inverted microscope. The polarization of the incident light is controlled by a linear polarizer, installed prior to a beam splitter, before the light is focused onto the sample using a 50× magnification, 0.8 numerical aperture (NA), 1 mm working distance microscope objective. The microscope provides an additional 1.5× magnification for a total of 75× magnification. The sample is mounted onto an XY (in-plane) piezoelectric translation stage (positional accuracy <1 nm) to assist with optimization of the in-coupling efficiency. The light from the sample is imaged via the same objective where it passes through the beamsplitter to a detector. The detector is a PHOTOMETRICS −70 °C cooled vacuum-sealed linear electron multiplying charge-coupled device (EMCCD) with a 512 × 512 pixel array $(16\ \mu m)^2$. The EMCCD gain is set to 0 to maximize the dynamic range of the image and maintain its linearity response. The spot size of the focused laser beam is measured to have a fwhm of 1.1 μm, acquired from an image of the light reflected from a flat gold surface.

To verify the earlier 2D electric field calculations and also determine the nature of the propagating modes, we illuminate V-groove waveguides, both without SiO_2 (Figure 3c) and with a 2320 nm SiO_2 layer (Figure 3d), and capture the resulting images using a 50 ms exposure time with 25-frame averaging. The V-groove device without oxidation is seen to only support wedge-based modes with the beam focus set close to the surface plane. As the focal plane is moved deeper into the groove, the wedge-mode pair disappears and no clear single intensity peak can be found. However, the V-groove device with the SiO_2 layer shows a clear single intensity peak as the focus is located deeper within the groove, in agreement with the calculations represented in Figure 2. Wedge-based modes may still be observed in the device with the SiO_2 layer, also in agreement with calculations, but they are considerably weaker than those exhibited by the device without the SiO_2 layer. To further investigate the single intensity peak, we rotate the incident polarization by 90° (Figure 3e) and observe close to a factor of 10 reduction in the relative intensity of out-coupled light. This out-coupled light is degenerate about the V-groove axis and supports the assumption that the waveguide mode is a V-groove CPP with a predominantly TE-polarization of the electric field (i.e., parallel to the surface plane and perpendicular to the groove axis) with a very weak longitudinal component.[36,38]

dx.doi.org/10.1021/nl5002058 | *Nano Lett.* XXXX, XXX, XXX–XXX

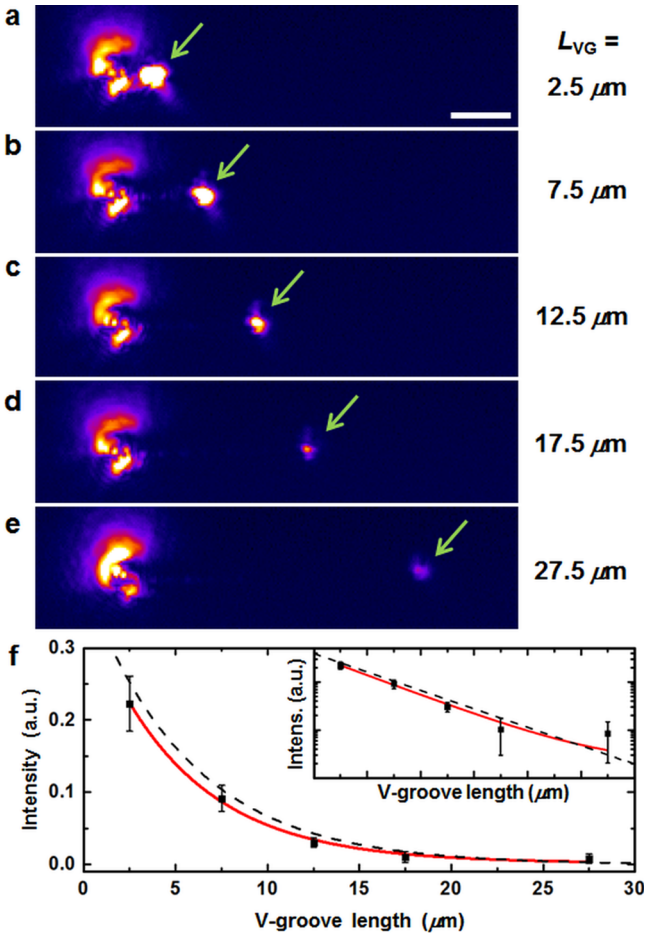

Figure 4. (a–e) The experimentally observed out-coupled light for varying V-groove lengths, L_{VG} with 2320 nm SiO_2 thickness. The incident light polarization is perpendicular to the V-groove axis. The white scale bar represents 5 μm and the normalized intensity scales similar to Figure 4. (f) Integrated output intensities as a function of V-groove waveguide length: data (black squares), exponential fit of the measurement (red solid line) and calculated values (black dashed line). The errors bars from the measurement represent the fwtm experimental error. Inset: semilog plot of the same data, indicating the increased relative error for longer V-grooves owing to decreasing SNR.

In order to find the propagation length of the V-groove CPPs, and hence the in-coupling and out-coupling efficiencies, we measure the ratio of the out-coupled power over the incident power, P_o/P_i, for varying V-groove lengths. We first measure the incident power by acquiring an image of the laser beam focused on and reflected from a flat gold surface and integrating the pixel values over a region wholly containing the laser spot. Likewise, the output power is measured using an integration region wholly containing the out-coupled signal. The background signal offset is removed by subtracting the power values in the integration windows while the laser source is turned off. To achieve maximum coupling efficiency, the incident light spot is positioned and focused accurately onto the termination mirror, determined by translating the piezoelectric stage and focal position until the out-coupled power, P_o, is maximized. In particular, the same focal plane is maintained relative to each termination mirror for the devices with different V-groove lengths by finding the optimal focus on a V-groove with large signal-to-noise ratio (SNR) and then translating the groove aside by 5 μm to obtain the incident spot size on the

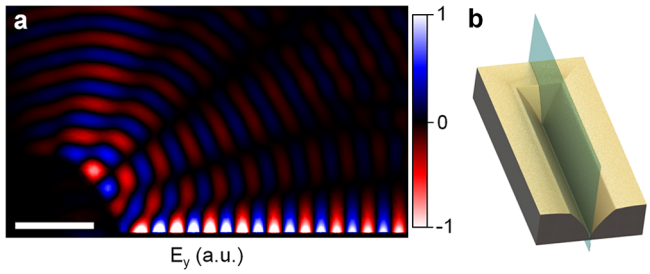

Figure 5. (a) Electric field slice plot of a 3D FEM simulation showing CPP excitation via normal illumination of a V-groove waveguide termination mirror with a Gaussian beam of spot size 1.1 μm. The V-groove and waveguide termination profiles have been modified by a 2320 nm SiO_2 layer similar to Figure 2d. The scale bar is 2 μm. (b) Illustration of the simulation geometry showing the slice used for the plot in (a).

adjacent flat section. Reversing this procedure, first adjusting the focus on a 5 μm-adjacent section to obtain the previously obtained spot size, then ensures the same relative focal plane is achieved for subsequent V-groove devices to be investigated.

Figure 4a–e shows a set of experimental images used for determining the P_o/P_i ratios of the varying V-groove lengths, L_{VG}. The values of L_{VG}, measured by SEM and excluding the mirrors, are 2.5, 7.5, 12.5, 17.5, and 27.5 μm. The length of each mirror, affected by the thermal SiO_2 growth process, is approximately 1.6 μm. All optical measurements are performed with the incident electric field oriented perpendicular to the waveguide axis. The integrated output intensities are plotted as a function of V-groove waveguide length in Figure 4f. The data is fitted with an exponential decay curve where the intensity propagation length is found to be 5.2 ± 0.1 μm. For comparison, the curve corresponding to the calculated propagation length from 2D FEM simulations is plotted on the same graph. The error bars represent the full width at tenth-maximum (fwtm). A semilog plot of the same data is included in the inset, indicating the increased relative error for longer V-grooves due to the decreasing SNR.

To determine the coupling efficiencies of our devices under direct illumination, we numerically calculate the optical behavior using 3D FEM simulations. In order to represent the experiment, the freely propagating light at λ_0 = 811 nm is defined with a Gaussian beam of 1.1 μm spot size impinging on a termination mirror of a V-groove device with SiO_2 thickness 2320 nm. The resulting solution that considers the in-coupling mirror is shown in Figure 5a, taken as the slice along the V-groove axis normal to the sample surface (Figure 5b). We evaluate the in-coupling efficiency as the ratio of the Poynting vector along the V-groove waveguide, integrated over the CPP mode distribution in the groove (P_{CPP}), to the Poynting vector normal to the device integrated over the laser beam (P_i). We find an in-coupling efficiency of η_i = 51.7%. We attribute the calculated 5-times increase of in-coupling efficiency over previous nanomirror results[36] to the larger mirror collection region and favorable curved profile caused by the SiO_2 layer. This is despite the negative effect caused by the average mirror angle being steeper than the 45° optimum[36] and that the convex shape varies this angle yet further away for the region close to the V-groove bottom.

To determine the out-coupling efficiency, we perform calculations for a system with both termination mirrors and find the Poynting vector of the light out-coupled from the mirror perimeter integrated within the NA determined by the

dx.doi.org/10.1021/nl5002058 | Nano Lett. XXXX, XXX, XXX–XXX

Table 1. Summary of Calculated versus Measured Coupling Efficiencies and Propagation Lengths

	prop. length, α	in-coupling, η_i	product, η	out-coupling, η_o
calculated	5.7 μm	51.7%	39.2%	75.9%
measured	5.2 ± 0.1 μm	51.4 ± 0.7%	35.8 ± 0.4%	75.5 ± 1.0%

microscope objective (P_o). A reference calculation is performed without the out-coupling mirror to remove scattered components that propagate outside the NA. We find an efficiency product, $\eta = \eta_i\eta_o$, of 39.2% and, therefore, an out-coupling efficiency of η_o = 75.9%. We attribute the fact that this value for η_o is lower than total out-coupling due to deviation of the mirror profile away from being flat and inclined at 45°, causing a portion of the out-coupled light to emit outside the microscope objective's cone of acceptance.

The measurements shown in Figure 4 yield an experimental mirror efficiency product of 35.8 ± 0.4%, which is an 8.8% decrease from the calculation. After accounting for the experimental reduction in propagation length, 5.2 μm versus 5.7 μm via calculation, and applying the remaining experimental decrease evenly to the two mirrors, an estimate for the experimental efficiency each mirror can be found, being η_i = 51.4% and η_o = 75.5%. The experimental value will slightly overestimate the total out-coupled power due to the imperfect reflectance of the flat gold surface used for taking reference measurements, although this value is not expected to decrease the value of the mirror coupling efficiencies by more than a percentage point since the absorption of gold at our operating wavelength is very low. The large in-coupling efficiency of the experiments, in addition to the reasons mentioned above for the calculation, are attributed to the smooth gold surface facilitated by the crystallographic etch and thermal SiO_2 growth processes. The calculated, measured, and estimated values for the mirror coupling efficiencies are summarized in Table 1.

In summary, we have demonstrated the efficient and convenient in-coupling of normally incident, freely propagating light to gold V-groove CPPs via compact 1.6 μm-length (5.2 μm^2 planar area) waveguide termination mirrors. Our measurements and calculations have shown in-coupling efficiencies over 50% and out-coupling efficiencies over 75%, representing remarkably high values that compare favorably with state-of-the-art demonstrations. In addition, the sample fabrication, involving conventional UV-lithography and crystallographic silicon etching, avoids the necessity of high-cost, serial writing techniques such as FIB or EBL to form high quality plasmonic structures. Furthermore, the fabrication process forms smooth termination mirrors inherent to the crystallographic etch step and paves the way toward parallel, wafer-scale production of devices that are both effective and straightforward to use. The V-shaped profiles formed by the silicon crystal planes, initially beyond the regime for supporting the desired CPP modes, are tailored by thermal SiO_2 growth to allow the V-grooves to support CPPs suitable for integration in highly confined nanophotonic systems. The wedge modes, while beyond the scope of this Letter, exhibit unique properties in their own right with propagation lengths up to 40 μm, also tailorable by thermal SiO_2 growth, and they exist in both the symmetric and antisymmetric electric field orientation configurations. The crystallographic formation of V-grooves, previously noted for being unable to form curved waveguides,[25] should nevertheless be able to form right-angled turns, which would open up new possibilities for deploying the V-groove waveguides in more sophisticated systems and is especially interesting considering the V-groove CPPs have been shown to propagate around sharp bends with minimal losses.[19] Finally, we remark that the coupling configuration of this work is especially ideal for efficient excitation of plasmonic elements collinearly through a microscope objective, such as for integrated lab-on-a-chip devices, or for facilitating efficient inter- and intrachip communication in planar or multileveled photonic information processing systems.

AUTHOR INFORMATION

Corresponding Author

*E-mail: anders.kristensen@nanotech.dtu.dk.

Author Contributions

C.L.C.S., A.H.T., C.E.G.-O., I.P.R., S.I.B., and A.K. conceived the experiments. C.L.C.S., A.H.T., C.E.G.-O., I.P.R., R.M., and C.V. performed the experiments. C.L.C.S. and A.H.T. performed the thermal SiO_2 layer geometry models and 2D FEM simulations in COMSOL. C.L.C.S., C.J., and C.V. performed the 3D FEM simulations in COMSOL and, together with C.E.G.-O., I.P.R. and S.I.B., analyzed their results. The device fabrication procedure was conceived by C.L.C.S. and A.H.T.; C.L.C.S. performed the fabrication. C.L.C.S. with assistance from A.H.T. wrote the first draft of the manuscript. All coauthors contributed and have given approval to the final version of the manuscript.

Notes

The authors declare no competing financial interest.

ACKNOWLEDGMENTS

C.L.C.S. and C.V. acknowledge financial support from the Danish Council for Independent Research (FTP Grants 12-126601 and 12-126676). C.E.G.-O., I.P.R., and S.I.B. acknowledge financial support from the Danish Council for Independent Research (FTP project ANAP, Contract No. 09-072949). R.M. acknowledges support from the EU project Cell-O-Matic (Grant 278204) and the Danish Council for Strategic Research (Grant 10-092322). C.J. acknowledges financial support from the Danish Council for Independent Research (FTP project PCDC, Contract No. 10-082409).

REFERENCES

(1) Barnes, W. L.; Dereux, A.; Ebbesen, T. W. *Nature* **2003**, *424*, 824−830.

(2) Yin, L.; Vlasko-Vlasov, V. K.; Pearson, J.; Hiller, J. M.; Hua, J.; Welp, U.; Brown, D. E.; Kimball, C. W. *Nano Lett.* **2005**, *5*, 1399−1402.

(3) Verhagen, E.; Polman, A.; Kuipers, L. K. *Opt. Express* **2008**, *16*, 45−57.

(4) Schuller, J. A; Barnard, E. S.; Cai, W.; Jun, Y. C.; White, J. S.; Brongersma, M. L. *Nat. Mater.* **2010**, *9*, 193−204.

(5) Gramotnev, D. K.; Bozhevolnyi, S. I. *Nat. Photonics* **2010**, *4*, 83−91.

(6) Dionne, J.; Sweatlock, L.; Atwater, H.; Polman, A. *Phys. Rev. B* **2006**, *73*, 1−9.

(7) Oulton, R. F.; Sorger, V. J.; Genov, D. A.; Pile, D. F. P.; Zhang, X. *Nat. Photonics* **2008**, *2*, 496−500.

(8) Goykhman, I.; Desiatov, B.; Levy, U. *Appl. Phys. Lett.* **2010**, *97*, 141106.
(9) Zia, R.; Schuller, J.; Brongersma, M. *Phys. Rev. B* **2006**, *74*, 165415.
(10) Quinten, M.; Leitner, A.; Krenn, J. R.; Aussenegg, F. R. *Opt. Lett.* **1998**, *23*, 1331−1333.
(11) Ebbesen, T. W.; Genet, C.; Bozhevolnyi, S. I. *Phys. Today* **2008**, *61*, 44−50.
(12) Gramotnev, D. K.; Nielsen, M. G.; Tan, S. J.; Kurth, M. L.; Bozhevolnyi, S. I. *Nano Lett.* **2012**, *12*, 359−363.
(13) Wang, K.; Schonbrun, E.; Steinvurzel, P.; Crozier, K. B. *Nano Lett.* **2010**, *10*, 3506−3511.
(14) Erickson, D.; Serey, X.; Chen, Y.-F.; Mandal, S. *Lab Chip* **2011**, *11*, 995−1009.
(15) Maragò, O. M.; Jones, P. H.; Gucciardi, P. G.; Volpe, G.; Ferrari, A. C. *Nat. Nanotechnol.* **2013**, *8*, 807−819.
(16) Bozhevolnyi, S.; Volkov, V.; Devaux, E.; Ebbesen, T. *Phys. Rev. Lett.* **2005**, *95*, 1−4.
(17) Pile, D. F. P.; Gramotnev, D. K. *Opt. Lett.* **2005**, *30*, 1186−1188.
(18) Moreno, E.; Garcia-Vidal, F. J.; Rodrigo, S. G.; Martin-Moreno, L.; Bozhevolnyi, S. I. *Opt. Lett.* **2006**, *31*, 3447−3449.
(19) Bozhevolnyi, S. I.; Volkov, V. S.; Devaux, E.; Laluet, J.-Y.; Ebbesen, T. W. *Nature* **2006**, *440*, 508−511.
(20) Volkov, V. S.; Bozhevolnyi, S. I.; Devaux, E.; Laluet, J.-Y.; Ebbesen, T. W. *Nano Lett.* **2007**, *7*, 880−884.
(21) Volkov, V. S.; Gosciniak, J.; Bozhevolnyi, S. I.; Rodrigo, S. G.; Martín-Moreno, L.; García-Vidal, F. J.; Devaux, E.; Ebbesen, T. W. *New J. Phys.* **2009**, *11*, 113043.
(22) Volkov, V. S.; Bozhevolnyi, S. I.; Rodrigo, S. G.; Garcı, F. J.; Ebbesen, T. W.; Alle, N. B. *Nano Lett.* **2009**, 1278−1282.
(23) Nielsen, R. B.; Fernandez-Cuesta, I.; Boltasseva, A.; Volkov, V. S.; Bozhevolnyi, S. I.; Klukowska, A.; Kristensen, A. *Opt. Lett.* **2008**, *33*, 2800−2802.
(24) Fernandez-Cuesta, I.; Nielsen, R. B.; Boltasseva, A.; Borrisé, X.; Pérez-Murano, F.; Kristensen, A. *J. Vac. Sci. Technol., B* **2007**, *25*, 2649−2653.
(25) Smith, C. L. C.; Desiatov, B.; Goykmann, I.; Fernandez-Cuesta, I.; Levy, U.; Kristensen, A. *Opt. Express* **2012**, *20*, 5696−5706.
(26) Kosako, T.; Kadoya, Y.; Hofmann, H. F. *Nat. Photonics* **2010**, *4*, 312−315.
(27) Curto, A. G.; Volpe, G.; Taminiau, T. H.; Kreuzer, M. P.; Quidant, R.; van Hulst, N. F. *Science* **2010**, *329*, 930−933.
(28) Kriesch, A.; Burgos, S. P.; Ploss, D.; Pfeifer, H.; Atwater, H. A; Peschel, U. *Nano Lett.* **2013**, 4539−4545.
(29) Aieta, F.; Genevet, P.; Kats, M. A; Yu, N.; Blanchard, R.; Gaburro, Z.; Capasso, F. *Nano Lett.* **2012**, *12*, 4932−4396.
(30) Vercruysse, D.; Sonnefraud, Y.; Verellen, N.; Fuchs, F. B.; Di Martino, G.; Lagae, L.; Moshchalkov, V. V; Maier, S. A; Van Dorpe, P. *Nano Lett.* **2013**, 3843−3849.
(31) Esslinger, M.; Khunsin, W.; Talebi, N.; Wei, T.; Dorfmüller, J.; Vogelgesang, R.; Kern, K. *Adv. Opt. Mater.* **2013**, 434−437.
(32) Esteban, R.; Teperik, T. V.; Greffet, J. J. *Phys. Rev. Lett.* **2010**, *104*, 026802.
(33) Qu, S.-W.; Nie, Z.-P. *Sci. Rep.* **2013**, *3*, 3172.
(34) Choi, S. B.; Park, D. J.; Jeong, Y. K.; Yun, Y. C.; Jeong, M. S.; Byeon, C. C.; Kang, J. H.; Park, Q.-H.; Kim, D. S. *Appl. Phys. Lett.* **2009**, *94*, 063115.
(35) Baron, A.; Devaux, E.; Rodier, J.-C.; Hugonin, J.-P.; Rousseau, E.; Genet, C.; Ebbesen, T. W.; Lalanne, P. *Nano Lett.* **2011**, *11*, 4207−4212.
(36) Radko, I. P.; Holmgaard, T.; Han, Z.; Pedersen, K.; Bozhevolnyi, S. I. *Appl. Phys. Lett.* **2011**, *99*, 213109.
(37) http://www.silvaco.com/products/tcad/process_simulation/athena/athena.html (accessed January 9, 2014).
(38) Bozhevolnyi, S. I.; Nerkararyan, K. V. *Opt. Lett.* **2009**, *34*, 2039−2041.